



Electrochemical activation of carbon–halogen bonds: Electrocatalysis at silver/copper nanoparticles



Christian Durante, Valentina Perazzolo, Lorenzo Perini, Marco Favaro,
Gaetano Granozzi, Armando Gennaro*

Department of Chemical Sciences, University of Padova, Via Marzolo, 1, 35131 Padova, Italy

ARTICLE INFO

Article history:

Received 13 January 2014

Received in revised form 11 April 2014

Accepted 14 April 2014

Available online 21 April 2014

Keywords:

Nanoparticles

Electrocatalysis

Silver

Copper

Organic chlorides

ABSTRACT

Cu nanoparticles (NPs) of average dimension of 20–30 nm were deposited following a double step potential deposition on glassy carbon (GC). Cu NPs morphology, shape, dimension and distribution were investigated by scanning electron microscopy (SEM). According to SEM the electrochemical deposition of Cu produces two different type of NPs (spherical and polyhedral), which result randomly distributed all over the GC support. In a second step, Ag was deposited over Cu NPs by displacement deposition giving a Cu nanostructured electrode decorated with very small Ag NPs (hereafter Ag/Cu). The electrodes were fully characterized by X-ray photoemission spectroscopy and energy dispersive X-ray spectroscopy, which provided the surface and bulk chemical composition of the electrodes.

The reductive cleavage of a series of organic chlorides, including chloroaromatics, benzyl chlorides, trichloroethylene and polychloromethanes, was investigated both at Cu and Ag/Cu NPs in DMF + 0.1 M (C₂H₅)₄NBF₄. Cu and Ag/Cu NPs electrodes have shown remarkable electrocatalytic reduction properties for the halides following concerted dissociative electron transfer. The peak potentials recorded at Cu and Ag/Cu NPs electrodes at $\nu = 0.2 \text{ V s}^{-1}$ are positively shifted by 0.3–0.5 V with respect to the reduction potentials measured at a non-catalytic electrode such as GC and in some cases the catalytic effect is even better than bulk Ag and Cu.

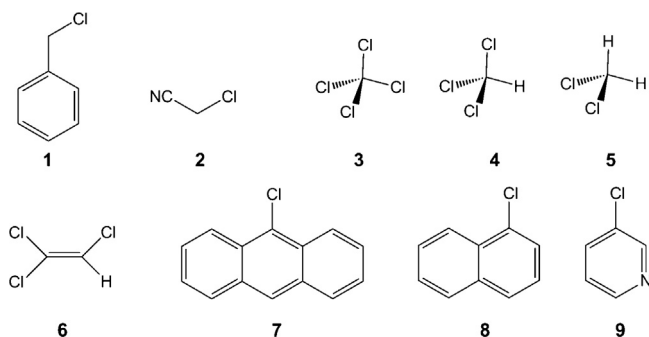
© 2014 Elsevier B.V. All rights reserved.

1. Introduction

Halogenated organic compounds represent one of the most important class of molecules employed in organic synthesis both as reagents and solvents. This is particularly true in the case of organic chlorides, since they are easily affordable and on hand. The efficient formation of carbon–carbon bonds is the most challenging aspect of the organic synthesis and innumerable examples can be found in the literature or in text books as well, where organic chloride or bromides are employed in coupling [1,2], carboxylation [3,4] cyclization [5] and polymerization reactions [6,7]. These are just few examples for emphasizing the huge quantity of chemicals that every passing minutes are processed for affording useful drugs, material or products for the everyday life. The other side of the coin is that a variegated range of waste with stable chemical properties and toxicity is produced. In fact, organic

chlorides cannot undergo an easy and fast natural degradation and this put some concern on their disposal and treatment. The degradation or conversion of organic chlorides is usually based on the reductive hydrodehalogenation reaction. However, because of the relatively high dissociation energy of C–Cl bond, catalysts are needed: the hydrodehalogenation process is usually mediated by a transition-metal catalyst, such as Pd or Fe under hydrogen pressure [8,9] or by microbial methods [10,11]. Besides to chemical or biological methods, the electrochemical approach is becoming a valid alternative. In fact, electrocatalysis can be successfully employed either in organic electrosynthesis [12,13] or in degradation or conversion of halogenated pollutants to less harmful and possibly more valuable compounds [14,15]. This has boosted over the last decade the research of electrode materials active toward the C–X bond breaking, and, so far, Ag [16–19], Cu [20–22] and Pd [23,24], and some of their combinatorial alloys [25,26] were found to possess interesting electrocatalytic properties. However, despite nano-catalysts have emerged as a sustainable and competitive alternative in recent years, there are very few examples in the literature reporting the employments of NPs decorated electrodes

* Corresponding author. Tel.: +39 049 8275132; fax: +39 049 8275829.
E-mail address: armando.gennaro@unipd.it (A. Gennaro).



Scheme 1.

in the field of C–X bond activation and the most of them are based on Ag NPs [16,23,27–30]. Actually, a fine dispersion of the metal NPs and/or the modulation of their electronic properties by interaction with support chemical or morphological defects may increase the catalytic activity and selectivity [23]. Furthermore, because of the high surface-to-volume ratio it is possible to obtain high current density despite a low loading of active phase, thus enhancing the efficiency while decreasing the reaction time and the process costs.

In this paper we have investigated the electrochemical deposition of Cu and mixed Ag/Cu NPs on glassy carbon (GC). GC has been chosen as electrode support since among various forms of carbon, it is an optimal material for a basic investigation of the catalytic activity of the loaded catalyst, minimizing the possible morphological and/or chemical effects of the support. In fact, GC is generally considered an inert material with respect to halogen reduction [31], it possesses very low electrical resistivity and it is non-porous and impermeable to gases [32]. Furthermore, it can be easily polished and managed allowing a good reproducibility among different experiments. Copper NPs have been chosen as an electroactive phase alternative to Ag NPs in the reduction of organic halides. Actually, Cu electrodes have been found to possess good electrocatalytic properties for the reduction of alkyl bromides, iodides and chlorides [33,34,24,22] but there is no report in the literature confirming such activity also for Cu NPs. Furthermore, Cu has the advantages of excellent electrical conductivity (only 6% less than that of Ag) and much lower price. On the other hand, Cu NPs oxidizes rapidly under ambient conditions and this can put a severe limit to their practical application. A viable strategy to overcome the problem is the introduction of a second metal, which can improve the oxidation resistance. In this sense, Cu NPs with Ag coating appear a promising material to be employed in electrocatalysis [35,36], and by limiting the more expensive and reactive metal Ag to the surface of the NPs a substantial saving is possible. Ag/Cu NPs were prepared via a cheap and convenient method: Cu NPs are preliminary deposited on GC and then plated with Ag by a displacement reaction with a silver salt. Therefore the aim of this study is to understand whether the electrocatalytic activities of these nanostructured electrodes can approach or even outclass those of the relative bulk materials. The Cu and Ag/Cu nanostructured electrodes were fully characterized by X-ray photoemission spectroscopy (XPS), scanning electron microscopy (SEM) and energy dispersive X-ray spectroscopy (EDX), while the electrochemical reactivity was tested toward the reduction of a series of different organic chlorides, including benzyl chloride, which so far is considered as a benchmark molecule for investigating the carbon-halogen bond activation (Scheme 1). The other selected compounds allow examination of the effect of molecular structure on the electrocatalytic properties.

2. Experimental

2.1. Chemicals

Dimethylformamide (DMF) (Prolabo ≥ 99.8) was kept over anhydrous Na_2CO_3 for several days and stirred from time to time. It was then fractionally distilled twice under reduced pressure and stored in a dark bottle under argon. Tetraethylammoniumtetrafluoroborate (TEABF₄, Fluka, 98%) was recrystallized twice from absolute EtOH and dried in a vacuum oven at 70 °C. The deionized water used for the experiments was previously bi-distilled in the presence of KMnO_4 . All other reagents were commercially available with good purity and were used without further purification.

2.2. Instrumentation

The morphological characterization of Cu and Ag/Cu nanoparticles deposited onto GC was performed by field emission scanning electron microscopy (Zeiss Supra 35 VP).

The XPS characterization of the samples was performed in an UHV chamber (base pressure $<5 \times 10^{-9}$ mbar), equipped with a double anode X-ray source (Omicron), a hemispherical electron analyzer (VG Scienta). All the XPS measurements were performed at room temperature, using non-monochromatized Mg-K α radiation ($h\nu = 1253.6$ eV) and a pass energy of 50 eV and 20 eV for the survey and high-resolution spectra, respectively. The calibration of the binding energy (BE) scale was carried out using Au 4f as reference (BE = 84 eV).

Electrochemical experiments were performed at 25 °C by using an Autolab PGSTAT100 N potentiostat/galvanostat. The electrocatalytic activity of the nanostructured surfaces for organic chloride reduction was investigated using cyclic voltammetry (CV) and were carried out in a three-electrode cell system with a GC, either modified or unmodified, or Ag and Cu disc as working electrode. The working electrodes for cyclic voltammetry were embedded in glass or Peek and were built from a 3 mm diameter GC rod (Tokai GC-20) or from a 2 mm diameter Ag or Cu wire (Alfa Aesar, 99.999%) and were polished to a mirror finish with silicon carbide papers of decreasing grain size (Struers, grit: 800, 2400, 4000) followed by diamond paste (3-, 1-, 0.25- μm particle size). They were then cleaned in ethanol in an ultrasonic bath for about 5 min. Prior to each experiment the electrode surfaces were refreshed by polishing with a 0.25 μm diamond paste, followed by ultrasonic rinsing [37]. The counter and reference electrodes were a Pt wire and Ag|AgI|Bu₄NI 0.1 M in DMF, respectively. All potentials are reported versus the saturated calomel electrode (SCE). This has been achieved by calibrating the Ag|AgI|[−] reference system at the end of each experiment against the ferrocenium/ferrocene couple ($E_{\text{Fc}^+/\text{Fc}} = 0.476$ V vs. SCE in DMF) and converting the potentials to the SCE scale [38].

The Cu and Ag/Cu NPs were freshly prepared on GC, before recording each set of cyclic voltammeteries, by electrodeposition of Cu on an exposed area of 3 mm diameter GC disc. The electrochemical deposition of Cu NPs was carried out in a three-electrode cell system containing 5 mM $\text{CuSO}_4 + 0.1$ M LiClO_4 in H_2O . GC was set as working electrode, while the counter electrode and the reference electrode were a Pt wire and a $\text{Hg}|\text{Hg}_2\text{SO}_4|\text{K}_2\text{SO}_4$ saturated electrode, respectively. The reference electrode was separated by the working electrode compartment, through a salt bridge which avoided any contamination of the working electrode. The conversion of the potential measured versus $\text{Hg}|\text{Hg}_2\text{SO}_4|\text{SO}_4^{2-}$ to the SCE scale is obtained adding +0.373 V to the measured value. All experiments were carried out at 25 °C.

Underpotential deposition measurements on bulk and modified electrodes were carried out by CV in an oxygen free water solution

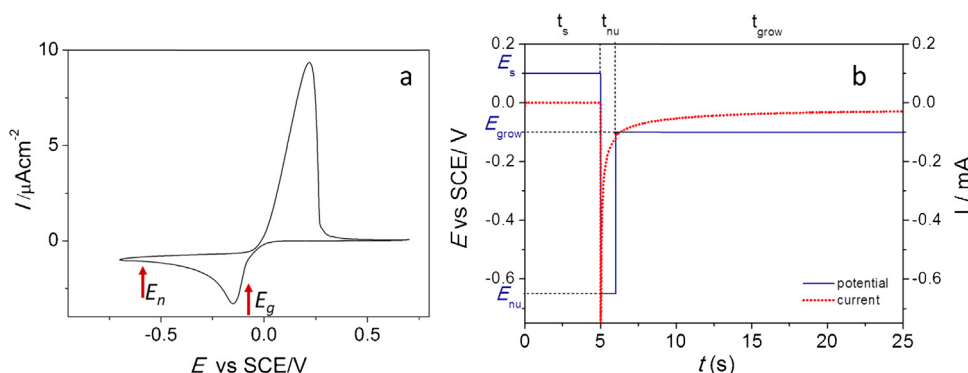


Fig. 1. (a) Cyclic voltammetry in $\text{H}_2\text{O} + 5 \text{ mM CuSO}_4 + 0.1 \text{ M LiClO}_4$ at GC, scan rate 0.2 V s^{-1} ; (b) Double potential pulse for the Cu deposition applied in this study.

containing $2 \text{ mM Pb(NO}_3)_2$ (99.9% metal basis, Carlo Erba) + 0.1 M HClO_4 (68% Fluka). SCE and Pt electrodes were used as reference and counter electrodes, respectively. The charge passed in such experiments was corrected for the background contribution assessing double-layer charging, by subtracting the charge recorded in the same solution but in the absence of Pb^{2+} ions.

3. Results and discussions

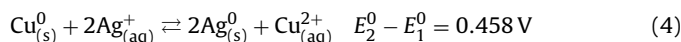
3.1. Preparation of Cu and Ag/Cu NPs

We have firstly investigated the redox reactions of copper on GC by CV in $\text{H}_2\text{O} + 5 \text{ mM CuSO}_4 + 0.1 \text{ M LiClO}_4$ solution; the resulting voltammogram is depicted in Fig. 1a. The voltammogram, starting from positive potential and going toward more negative values shows a diffusion controlled reduction peak with $E_p = -0.150 \text{ V}$ vs. SCE responsible for the reduction of Cu^{2+} to metal copper (Eq. (1)).



On the reverse scan a sharp oxidation peak is present at $E_p = 0.215 \text{ V}$ vs. SCE, where the dissolution of metal copper stuck on the electrode, upon its deposition during the forward scan, occurs. The charge for Cu deposition (both the forward and the reverse scan must be considered) and Cu stripping were integrated, resulting to be 7.43×10^{-3} and $7.35 \times 10^{-3} \text{ C}$, respectively. There are several examples in the literature reporting investigation on Cu deposition on GC electrode [39–43], however, Cu NPs electrochemically deposited on GC are much less investigated. In this work we have adopted a double potential step deposition of copper, since we have found this procedure really versatile also with other metals such as palladium [23] and because other different procedures attempted both in aqueous and organic solvent resulted quite unsatisfactory. In fact, this method allows a better control over the dimension and dispersion of metal NPs, since it is composed of independent nucleation and growing steps (Fig. 1b). In the present case, a pre-conditioning step was included before the two deposition steps in order to avoid any possible unwanted copper deposition and to strip away any copper traces possibly present on the GC surface. The preconditioning step was set at 0.25 V vs. SCE and held for 5 s. The first step (nucleation step) was set at a sufficiently negative potential ($E_{\text{nu}} = -0.65 \text{ V}$ vs. SCE) for 1 s allowing the deposition process to be controlled only by diffusion and, as a consequence, instantaneous nucleation of Cu took place. In the second step (growth step) the potential was set at $E_{\text{grow}} = -0.077 \text{ V}$ vs. SCE and held for 20 s. At this potential the process is kinetic-controlled and the Cu NPs grow without further nucleation of new sites. The solution was oxygen free and unstirred during the depositions. The deposition current was recorded and integrated in order to determine and compare the total deposition charge (Fig. 1 red line). From now on electrodes prepared in such a way will be referred as CuNPs-GC.

The silver/copper electrodes were prepared by employing CuNPs-GC as substrate via the electroless displacement of the less noble metal (Cu) by the more noble metal (Ag). The deposition bath was $\text{H}_2\text{O} + 0.4 \text{ mM AgNO}_3 + 0.1 \text{ M KNO}_3$ solution. The displacement deposition of Ag on Cu is a thermodynamically favored process since the resulting cell potential for the global reaction assumes a positive value $e.m.f. = 0.458 \text{ V}$ (Eqs. (2)–(4)).



This type of deposition is a non-equilibrium process since the deposition occurs at a potential between the equilibrium potential of the two redox couples, usually referred as mixed potential, which is far from the equilibrium potential.

3.2. Morphological and chemical characterization of Cu and Ag/Cu NPs

The morphological characterization of the samples by SEM after the electrochemical deposition of Cu shows the presence of Cu NPs, which appear homogeneously distributed all over the GC support (Fig. 2). A deposit formed with a growing step of 20 s shows well separated crystallites (Fig. 2a and b) presenting a bimodal distribution (Fig. 2c): polyhedral Cu NPs can be individuated as very small crystallites of average size of 23 nm, far more numerous than spherical Cu NPs, which are brighter and of bigger average dimension (46 nm). Different shape in metal NPs is usually the result of a preferential growth of planes with low surface free energy with respect to those with a high surface free energy [44]. The control over the shape of metal NPs is generally accomplished by choosing appropriate metal salt concentration, surfactant agents and by tuning the reduction potential [45,46]. In particular, cubic-polyhedral metal NPs are favored at low metal salt concentration ($<5 \text{ mM}$) and deposition potential lower than -0.1 V . In the present case, it is not clear whether one structure (spherical) is the evolution of the other (polyhedral); however, we may guess that the presence of two different crystallites is the result of nucleation sites of different nature, in term of morphology (surface defects) and surface chemistry (different oxygen functional groups), within the same GC support, being all the other conditions identical. SEM images of CuNPs-GC deposited with a growing step of 30 s are reported in Fig. 2d and e. Also in this case both polyhedral and spherical Cu NPs of average size of 30 and 65 nm are present and randomly distributed over the GC support. In this case it can be observed a decrease of the particle density distribution; in particular, there is a sensible diminution of small particles ($<20 \text{ nm}$) (Fig. 2e). This phenomenon is not surprising since it is well known

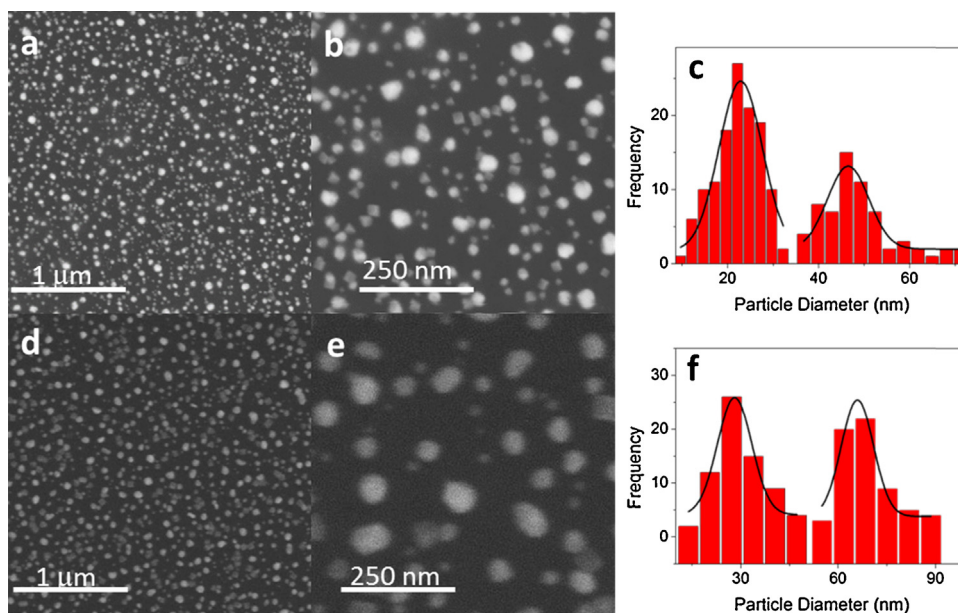


Fig. 2. SEM images at two different magnifications and particle size distributions for: (a–c) CuNPs-GC, $t_{\text{grow}} = 20$ s; (d–f) CuNPs-GC, $t_{\text{grow}} = 30$ s.

that the Gibbs free energy of cluster formation is inversely proportional to the applied overvoltage, thus while the formation of small clusters is favored at potential far more negative than the equilibrium potential, as it is the case of the nucleation step, the opposite effect is expected under controlled kinetic condition, i.e. during the growing step. The result is that the less stable small particles are inclined to aggregate or dissolve.

Fig. 3 shows the morphology evolution of CuNPs-GC growth for 20 s upon the galvanic displacement process in a 0.4 mM silver bath at two different deposition time: 150 s (**Fig. 3a** and **b**) and 600 s (**Fig. 3c** and **d**). The two samples will be referred from now on as Ag150@CuNPs-GC and Ag600@CuNPs-GC. The Ag displacement deposition appears as the formation of small Ag NPs (≈ 10 nm) over copper NPs resulting in the formation of mixed silver-copper aggregates of average dimension of 30 nm. Small NPs are evident in the sample Ag150@CuNPs-GC (**Fig. 3b**) whereas in Ag600@CuNPs-GC the average size of Ag/Cu increase to 40 nm.

It is well-proven in the literature that galvanic replacement of Cu with Ag leads to homogeneously covered Cu NPs, with the formation of core-shell systems [47,48]. At the beginning of the galvanic replacement reaction, the copper exchange is important and rapid at the surface of the NPs, until the saturation of all the surface copper atoms [47]. Then, it decreases and is almost stabilized after several minutes. Consequently, the thickness of the silver layer rises more slowly. These phenomena are easily explained by the coating of the copper surface: at the start, the entire sample surface is available for the displacement reaction (with the consequent formation of a core-shell system), but after some minutes, the exposed copper surface becomes so low that the Cu–Ag exchange greatly decreases. However, the electroless process may continue by Cu^{2+} transport through pores or grain boundaries or other diffusion paths of the growing Ag layer [47]. Moreover, on the sites of Cu NPs, where Cu^{2+} transport is more efficient (like along the edges of the Cu polyhedral NPs), the high galvanic exchange rate can produce very small Ag nuclei that can act as preferential sites for the further deposition of silver [48,49] which leads to the growth of Ag NPs on the edge sites of the Cu polyhedrons, as well-documented on a particularly big cubical Cu crystallite shown in **Fig. 3d**. A pictorial description of this phenomenology is reported in **Fig. 3e** and **f**.

The chemical characterization of Ag150@CuNPs-GC and Ag600@CuNPs-GC has been carried out by using both XPS and

EDX. The XPS surveys for the two samples, reported in **Fig. 4**, show the photoionization of the Ag 3d and Cu 2p core level (centred at 368.4 eV and 932.6 eV, respectively), while the C 1s (284.8 eV) and O 1s (532.3 eV) photoionization signals come from the GC support. The presence of the photoemission fluorine finger print in the spectral region between 590 eV and 720 eV (F 1s and Auger KLL series) is due to the fluorine contamination coming from the Teflon taped employed for delimiting the GC surface area during the sample preparation. The Ag peak intensity increases passing from Ag150@CuNPs-GC to Ag600@CuNPs-GC according to an increased amount of deposited Ag (**Fig. 4b**). The formation of several shells of Ag on Cu NPs, accordingly to the above described mechanism, is then in agreement with the results of XPS spectroscopy, where Ag signals are much more intense than those of Cu, also at the lowest loading. Since the photoionization cross section of Ag 3d is equal to 2/3 of that of Cu 2p, the observed phenomenology can be attributed only to the inelastic attenuation experienced by the Cu photoelectrons by the Ag overlayer: using Mg $K\alpha$, the inelastic mean free path of the Cu photoelectrons, attenuated by the Ag overlayer, is equal to 6.8 Å. Since the interplanar distance between two atomic (1 1 1) planes in Ag is 7.07 Å [50], it appears clear that only 1.5 monolayer equivalents of Ag over the Cu NP surface are enough to attenuate by more than 50% of the Cu signal coming from the underlying layers. However, a bulk-sensitive analysis such as EDX (performed in this work at an acceleration potential of the primary electrons equal to 10 keV), reveals a Ag/Cu ratio of 1/2 and 1/1 for Ag150@CuNPs-GC and Ag600@CuNPs-GC, respectively. This is indicative that though Ag is the main component of the electrode surface, Cu remain the principal element of the NPs. In order to investigate the oxidation state of the deposited silver, the calculation of the Auger parameter is necessary. In the early 1970s, Wagner first introduced the Auger parameter (α) [51,52] to study photoemission binding energy shifts [53,54] as:

$$\alpha = \text{BE}(x_i) + \text{KE}(x_i x_j x_k) \quad (5)$$

where $\text{BE}(x_i)$ is the core level (x_i) binding energy and $\text{KE}(x_i x_j x_k)$ is the kinetic energy of the Auger transitions from the x_i , x_j , and x_k core levels, respectively.

Using a Mg- $K\alpha$ source, Ag is characterized by an intense and sharp Auger M_4V_V (3d–4d, centered at 895.5 eV) transition [55], as it can be observed in **Fig. 4c**. Thence, by means of Eq. (5), we have

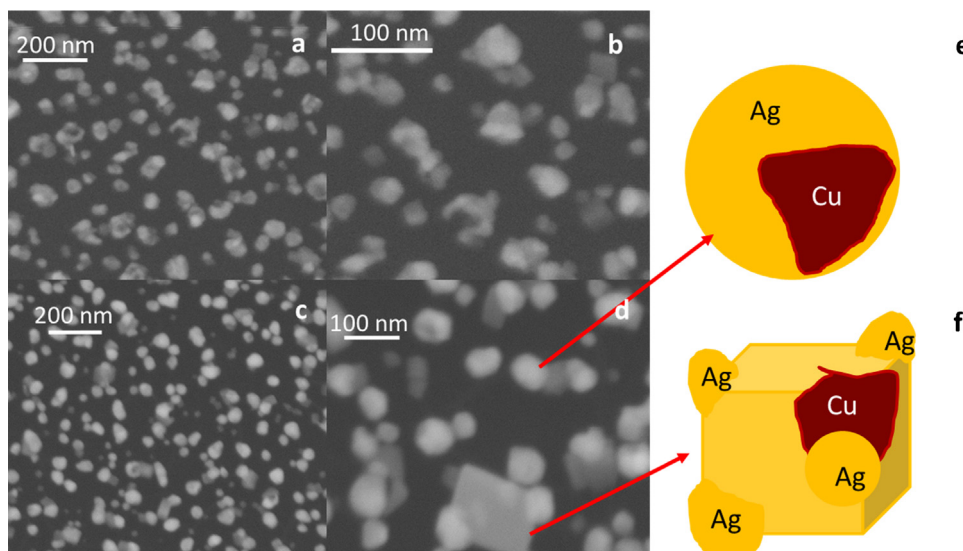


Fig. 3. SEM images at two different magnifications: (a,b) Ag150@CuNPs-GC; (c,d) Ag600@CuNPs-GC and (e,f) proposed model for Ag/Cu NPs.

calculated the α value for the two different Ag coverage, finding a value of 722.2 eV for both Ag150@CuNPs-GC to Ag600@CuNPs-GC. According to the literature [51], this value proves that the Ag deposited on the Cu NPs by galvanic displacement is in a zero-valent state (Ag^0). It has also to be stressed that it is not possible to discriminate if the Ag forms an alloy with Cu, because of the weak difference in the electronegativity that characterizes the two metals (1.93 and 1.91, respectively). Then, if the Ag is alloyed with Cu, the initial state effect will be negligible with respect of that relative to a system con-

stituted only by metallic Ag. This eventually results in a negligible shift of the Auger parameters that characterize the two different systems [56].

A very important parameter for a catalyst is the active surface area. The underpotential deposition (UPD) of a metal monolayer over a foreign substrate is a very reliable method for the estimation of real surface area and roughness of an electrode. In the present case Pb has been chosen for its ability to form a UPD layer on a variety of noble metals, including Ag [57] and Cu [58]. The procedure

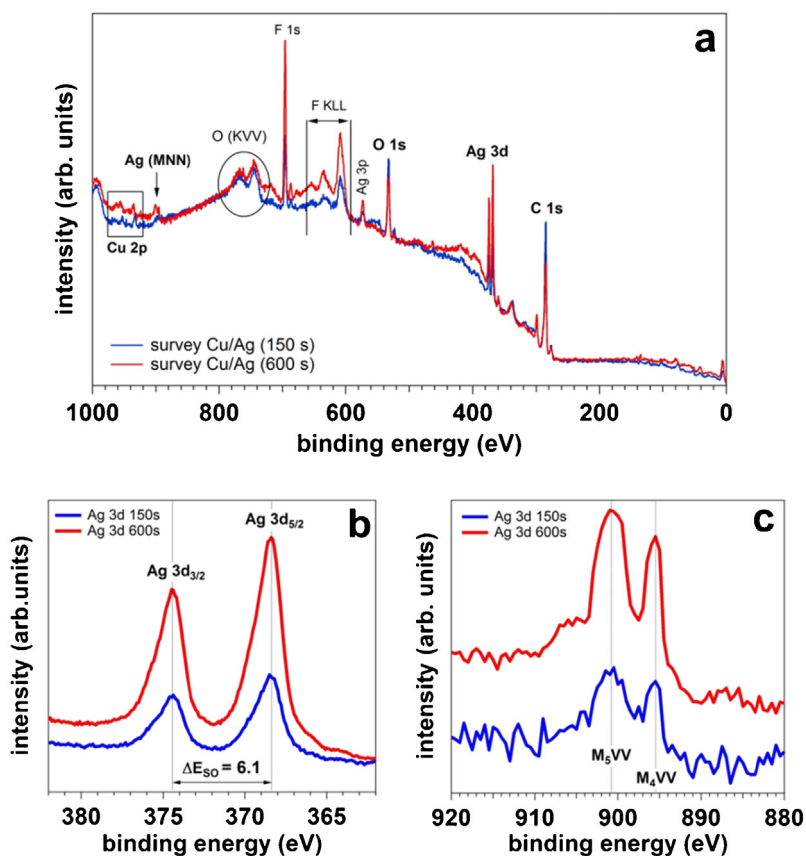


Fig. 4. XPS spectra of Ag150@CuNPs-GC and Ag600@CuNPs-GC: (a) XPS survey wide scans; (b) Ag 3d XPS peaks; (c) Ag Auger transition peaks.

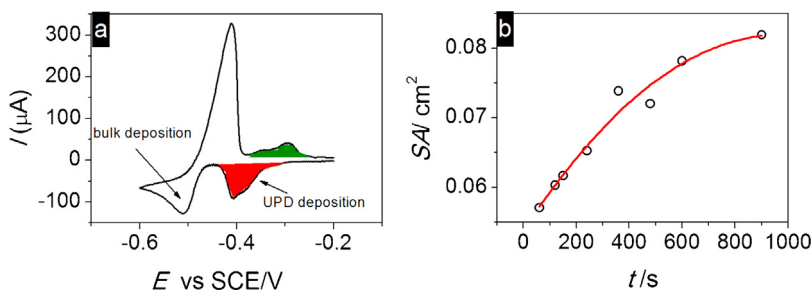


Fig. 5. a) Cyclic voltammetry of $\text{Pb}(\text{NO}_3)_2$ 2 mM in $\text{H}_2\text{O} + 0.1 \text{ M HClO}_4$ at Ag600@CuNPs-GC , scan rate 0.2 V s^{-1} ; (b) variation of the surface area of Ag/Cu nanostructured electrodes on the increase of Ag loading.

consists on the selective deposition of a full monolayer of Pb on Ag or Cu surface, the charge associate to the deposition/dissolution of the Pb monolayer is directly proportional to the substrate surface area and can be evaluated according to the ratio [59]:

$$A = \frac{Q_{\text{UPD}}}{q_m} \quad (6)$$

where Q_{UPD} is the charge consumed, which can easily be obtained by simply integrating the current density over time using either the CV formation or stripping curves, whereas q_m is the monolayer charge density and for Pb a common value is 0.390 mC cm^{-2} [60]. Pb UPD has been performed on Ag/Cu modified electrodes prepared on GC (geometric area 0.076 cm^2) and for sake of comparison also on a CuNPs-GC. Fig. 5a shows a CV performed on Ag600@CuNPs-GC , where it can be seen the presence of a Pb UPD peak at -0.4 V vs. SCE and a bulk deposition peak at -0.5 V vs. SCE. Since in the present condition, both Cu and Ag undergo Pb UPD we can estimate the whole active surface area. In particular the variation of the active surface should be affected by the increase of Ag loading. Therefore, Pb UPD analysis has been extended to a whole series of CuNPs-GC electrodes silvered at different Ag deposition time and the result is reported in Fig. 5b. It is interesting to note that the surface area increases by increasing the Ag deposition, reaching an almost constant value for $t > 15 \text{ min}$. In particular, CuNPs-GC, Ag150@CuNPs-GC and Ag600@CuNPs-GC have shown a surface area of 0.053, 0.060 and 0.078 cm^2 , respectively. Since upon Ag deposition the electrode surface area increases, the plot trend in Fig. 5b can be associated to the net variation of the electrode surface area upon the formation of small Ag NPs.

3.3. Electrocatalytic activity of Cu NPs and Ag/Cu NPs

The electrocatalytic activity of CuNPs-GC, Ag150@CuNPs-GC and Ag600@CuNPs-GC was tested for the reduction of benzyl chloride, that is often chosen as a model process for the electroreduction of organic halides. The mechanism of activation of organic halide is generally analyzed in the framework of dissociative electron transfer (DET) to C–X bonds. Whether the activation occurs at an inert or at a catalytic electrode, two reaction pathways are possible for the reductive cleavage of R-X to R^\bullet and X^- . These are a stepwise mechanism, involving an intermediate radical anion, $\text{R-X}^{\bullet-}$, which further decomposes to R^\bullet and X^- (Eqs. (7) and (8)) and a concerted mechanism, where electron transfer (ET) and bond breaking occur in a single step (Eq. (9)) [61,62]. Whichever of the two mechanism is followed, a R^\bullet radical is formed, that is generally more easily reducible than R-X and it readily undergoes a second ET (Eq. (10)). Therefore, the process involves two successive one-electron transfers leading to the carbanion R^- , which is then rapidly protonated by any proton donor BH present in solution (Eq. (11)).



A diagnostic criteria for asserting the one or the other mechanism is the determination of the kinetic indicator κ [62]. In the concerted mechanism, where the ET is the rate determining step (Eq. (7)), κ corresponds to the electron transfer coefficient α and it is typically much smaller than 0.5. In the stepwise mechanism κ takes into account for a mixed kinetic control, since both ET (Eq. (7)) and chemical reaction (Eq. (8)) limit the whole reaction rate; in this case values of $\kappa \geq 0.4$ are expected. The kinetic indicator κ can be determined by voltammetric analysis according to Eqs. (12) and (13), which are the equations for determining the ET coefficient α in the case of an irreversible ET [63]. If the peak potential E_p varies linearly with $\log \nu$, κ can be determined by the slope $\partial E_p / \partial \log \nu$ (Eq. (12)). Alternatively, κ can be calculated by Eq. (13), where $E_{p/2} - E_p$ is the peak width.

$$\frac{\partial E_p}{\partial \log \nu} = - \frac{1.151 RT}{\kappa F} \quad (12)$$

$$E_{p/2} - E_p = \frac{1.857 RT}{\kappa F} \quad (13)$$

The electrochemical behavior of benzyl chloride has extensively been investigated at both GC and metal electrodes and the reduction mechanism is so far well established. For this reason benzyl chloride is commonly employed as standard molecule in catalytic tests for the screening of novel electrode materials. The cyclic voltammetry of benzyl chloride on GC, Ag and Cu in DMF + TEABF₄ is reported in Fig. 6. According to the kinetic parameter $\kappa \ll 0.5$,

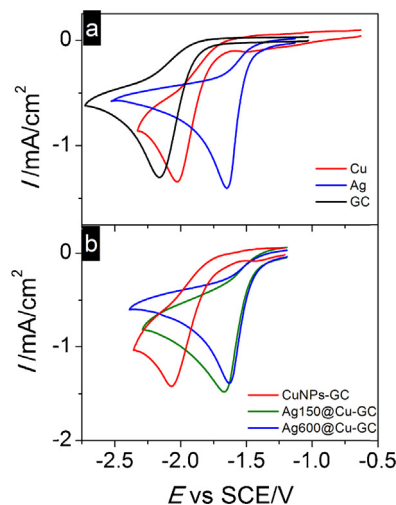


Fig. 6. Cyclic voltammetry of 2 mM benzyl chloride in DMF + 0.1 M TEABF₄ at $\nu = 0.2 \text{ V s}^{-1}$ (a) GC, Ag, Cu; (b) CuNPs-GC, Ag150@CuNPs-GC and Ag600@CuNPs-GC.

Table 1

Voltammetric data for benzyl chloride reduction (2 mM) in DMF + 0.1 M TEABF₄, measured at 0.2 V s^{−1} at bulk and nanostructured electrodes.

| Electrode | E_p^a (V) | $E_{p/2} - E_p$ (V) | I_p (μA) | κ^b | κ^c | ΔE_p^d (V) | A (cm ²) |
|----------------|-------------|---------------------|------------|------------|------------|--------------------|----------------------|
| GC | −2.153 | 0.144 | 99.4 | 0.32 | 0.33 | – | 0.071 ^e |
| Ag | −1.658 | 0.146 | 46.08 | 0.24 | 0.33 | 0.495 | 0.032 ^e |
| Cu | −2.086 | 0.122 | 40.32 | 0.33 | 0.39 | 0.067 | 0.032 ^e |
| CuNPs-GC | −2.068 | 0.175 | 92.61 | 0.32 | 0.27 | 0.085 | 0.053 ^f |
| Ag150@CuNPs-GC | −1.669 | 0.117 | 91.77 | 0.30 | 0.41 | 0.484 | 0.060 ^f |
| Ag600@CuNPs-GC | −1.631 | 0.134 | 101.47 | 0.34 | 0.35 | 0.522 | 0.078 ^f |

^a Potentials are referred to SCE.

^b Calculated from $\partial E_p / \partial \log v = -1.15 RT / \kappa F$.

^c Calculated from $E_{p/2} - E_p = 1.857 RT / \kappa F$.

^d $\Delta E_p = E_p^M - E_p^{GC}$.

^e Geometric area.

^f Real surface area.

determined in DMF + 0.1 M TEABF₄, it may be asserted that benzyl chlorides is reduced at GC, Ag and Cu following a concerted DET, as already observed in other different experimental conditions [24]. Benzyl chloride is reduced at −2.17 V at GC, which so far is considered a non-catalytic electrode. Actually, it has been observed that organic chlorides, following a concerted mechanism, show a peak potential shift (ΔE_p) when reduced at catalytic surface and thus ΔE_p can be conveniently considered a diagnostic parameter to quantify the electrocatalytic properties. The catalytic activity, expressed as $\Delta E_p = E_p^M - E_p^{GC}$, indicates that Ag and Cu exhibit an electrocatalytic effect of 0.495 V and 0.067 V, respectively (Table 1). A less evident catalytic activity of Cu with respect to Ag has already been observed in DMF + 0.1 M TEABF₄ for other compounds and it was found to be dependent from the type of organic chloride and proton availability [20].

Fig. 6b shows the electrochemical behaviour of benzyl chloride at CuNPs-GC, as a first example ever reported in literature of an organic chloride reduced on a nanostructured Cu electrode. The reduction peak has the typical features of a semi-infinite linear diffusive behaviour and occurs at a potential −2.07 V, value that is more positive than GC indicating that also Cu NPs possess a catalytic behaviour. In this case, Cu NPs show to be more performing than bulk Cu of almost 20 mV. Experiments performed on CuNPs-GC at higher Cu loading (Cu deposited for 30 s), with average NPs dimensions of 40–50 nm, show even better performances with $\Delta E_p = 0.13$ V. In this case it is difficult to establish whether the improved catalytic activity is an effect of the Cu loading or a size effect since one depends from the other.

Fig. 6b shows also the electrochemical behavior of benzyl chloride at Ag150@CuNPs-GC and Ag600@CuNPs-GC electrodes, which have values of $\kappa = 0.30$ and 0.34, respectively. Such values ascertain a concerted DET, as already observed at bulk Ag and Cu (Table 1). The most striking result is the catalytic performances observed in both cases notwithstanding the low Ag loading. In

fact, Ag150@CuNPs-GC and Ag600@CuNPs-GC show a potential shift $\Delta E_p = 0.484$ V and $\Delta E_p = 0.522$ V, respectively (Table 1). This suggests that the electrocatalytic activities of Ag are preserved and possibly even improved upon decreasing the loading and the dimensions of the metal down to particles of nanometric size.

In virtue of the promising results, the investigation on Cu and Ag/Cu nanostructured electrodes have been extended to a whole series of organic chlorides, with the aim to show whether the electrocatalytic activities of these materials is of general applicability. For a better comparison, we recorded cyclic voltammograms for the whole series of compounds at bulk Ag and Cu electrodes in the same conditions in which the data at Cu NPs and Ag/Cu NPs were obtained. The organic chlorides selected for the investigation (Scheme 1) possess different molecular structures, allowing the examination of DET mechanism effect on the electrocatalytic properties. The data obtained from the voltammetric analysis are collected in Tables 2 and 3, whereas some representative cyclic voltammetries are reported in Fig. 7.

According to the kinetic indicator κ listed in Table 2, chloroacetoneitrile (2) follows a concerted DET, and the positive shift of the peak potentials indicates a catalytic activity at Ag and Cu with respect to GC. Fig. 7a indicates that the catalytic activity is preserved also at CuNPs-GC, Ag150@CuNPs-GC and Ag600@CuNPs-GC electrodes and, according to the ΔE_p values reported in Table 3, it is even more higher than the corresponding bulk materials. Therefore, also in the case of chloroacetoneitrile the nanostructured electrodes works better than the bulk Ag and Cu.

Compounds (3)–(5) are polychlorinated compounds which undergo sequential reduction of each C–Cl bond up to complete hydrodehalogenation. Fig. 7c and d reports the electrochemical behavior of CHCl₃ as an example; at GC three reduction peaks are visible each for one reduction step, while at Cu and Ag only two peaks are present since in this case CH₂Cl₂ and CH₃Cl formed

Table 2

Voltammetric data for the reduction of organic chlorides (2 mM) in DMF + 0.1 M TEABF₄, at 0.2 V s^{−1} at GC and bulk metal electrodes.

| RCl | GC | | Ag | | | Cu | | |
|-----|-------------|------------|-------------|------------|--------------------|-------------|------------|--------------------|
| | E_p^a (V) | κ^b | E_p^a (V) | κ^b | ΔE_p^c (V) | E_p^a (V) | κ^b | ΔE_p^c (V) |
| 1 | −2.153 | 0.32 | −1.658 | 0.24 | 0.495 | −2.086 | 0.33 | 0.067 |
| 2 | −1.90 | 0.39 | −1.354 | 0.34 | 0.546 | −1.619 | 0.23 | 0.281 |
| 3 | −1.498 | 0.40 | −1.498 | 0.27 | 0.000 | −1.471 | 0.27 | 0.027 |
| 4 | −2.100 | 0.35 | −1.695 | 0.24 | 0.405 | −1.777 | 0.27 | 0.323 |
| 5 | −2.679 | 0.32 | −2.160 | 0.27 | 0.519 | −2.176 | 0.25 | 0.503 |
| 6 | −2.237 | 0.73 | −1.789 | 0.91 | 0.448 | −2.135 | 0.74 | 0.102 |
| 7 | −1.698 | 0.85 | −1.698 | 0.86 | 0.000 | −1.696 | 0.62 | 0.002 |
| 8 | −2.130 | 0.79 | −2.087 | 0.79 | 0.043 | −2.109 | 0.83 | 0.021 |
| 9 | −2.257 | 0.75 | −2.171 | 0.79 | 0.086 | −2.205 | 0.76 | 0.052 |

^a Potentials are referred to SCE.

^b Calculated from $\partial E_p / \partial \log v = -1.15 RT / \kappa F$.

^c $\Delta E_p = E_p^M - E_p^{GC}$.

Table 3

Voltammetric data for the reduction of organic chlorides (2 mM) in DMF + 0.1 M TEABF₄, at 0.2 V s⁻¹ at nanostructured electrodes.

| RCl | Cu20NPs-GC | | | Cu30NPs-GC | | | Ag150@ Cu20NPs-GC | | | Ag600@Cu20NPs-GC | | |
|-----|-------------|------------|--------------------|-------------|------------|--------------------|-------------------|------------|--------------------|------------------|------------|--------------------|
| | E_p^a (V) | κ^b | ΔE_p^c (V) | E_p^a (V) | κ^b | ΔE_p^c (V) | E_p^a (V) | κ^b | ΔE_p^c (V) | E_p^a (V) | κ^b | ΔE_p^c (V) |
| 1 | -2.068 | 0.33 | 0.085 | -2.026 | 0.18 | 0.127 | -1.669 | 0.30 | 0.484 | -1.631 | 0.34 | 0.522 |
| 2 | -1.594 | 0.33 | 0.306 | -1.613 | 0.30 | 0.287 | -1.350 | 0.30 | 0.550 | -1.301 | 0.34 | 0.599 |
| 3 | -1.476 | 0.26 | 0.022 | -1.444 | 0.19 | 0.054 | -1.490 | 0.27 | 0.008 | -1.475 | 0.23 | 0.023 |
| 4 | -1.865 | 0.26 | 0.235 | -1.868 | 0.26 | 0.232 | -1.740 | 0.28 | 0.360 | -1.700 | 0.3 | 0.385 |
| 5 | -2.202 | 0.29 | 0.477 | -2.199 | 0.28 | 0.480 | -2.190 | 0.27 | 0.489 | -2.146 | 0.27 | 0.533 |
| 6 | -2.092 | 0.23 | 0.145 | -2.084 | 0.16 | 0.153 | -1.839 | 0.15 | 0.398 | -1.793 | 0.17 | 0.444 |
| 7 | -1.695 | 0.87 | 0.003 | -1.698 | 0.84 | 0.000 | -1.700 | 0.74 | -0.002 | -1.700 | 0.76 | -0.002 |
| 8 | -2.091 | 0.80 | 0.039 | -2.105 | 0.69 | 0.025 | -2.090 | 0.78 | 0.040 | -2.085 | 0.78 | 0.045 |
| 9 | -2.169 | 0.67 | 0.088 | -2.233 | 0.63 | 0.024 | -2.191 | 0.59 | 0.066 | -2.181 | 0.63 | 0.076 |

^a Potentials are referred to SCE.

^b Calculated from $\partial E_p / \partial \log \nu = -1.15 RT / \kappa F$.

^c $\Delta E_p = E_p^M - E_p^{GC}$.

in situ are reduced at similar reduction potential [21]. Both Ag and Cu have already shown a catalytic ability in the reduction of polychloromethanes, especially in the presence of a proton source [20]. This was confirmed also at nanostructured Cu and Ag/Cu electrodes, where ΔE_p increases on the decrease of the number

of C–Cl bond, the sequence of the electrocatalytic activity being $\text{CCl}_4 < \text{CHCl}_3 < \text{CH}_2\text{Cl}_2$.

Trichloroethylene (**6**) is a polychlorinated vinyl compound widely investigated because it is an environmental threat. The reduction mechanism in aprotic environment consists in a α ,

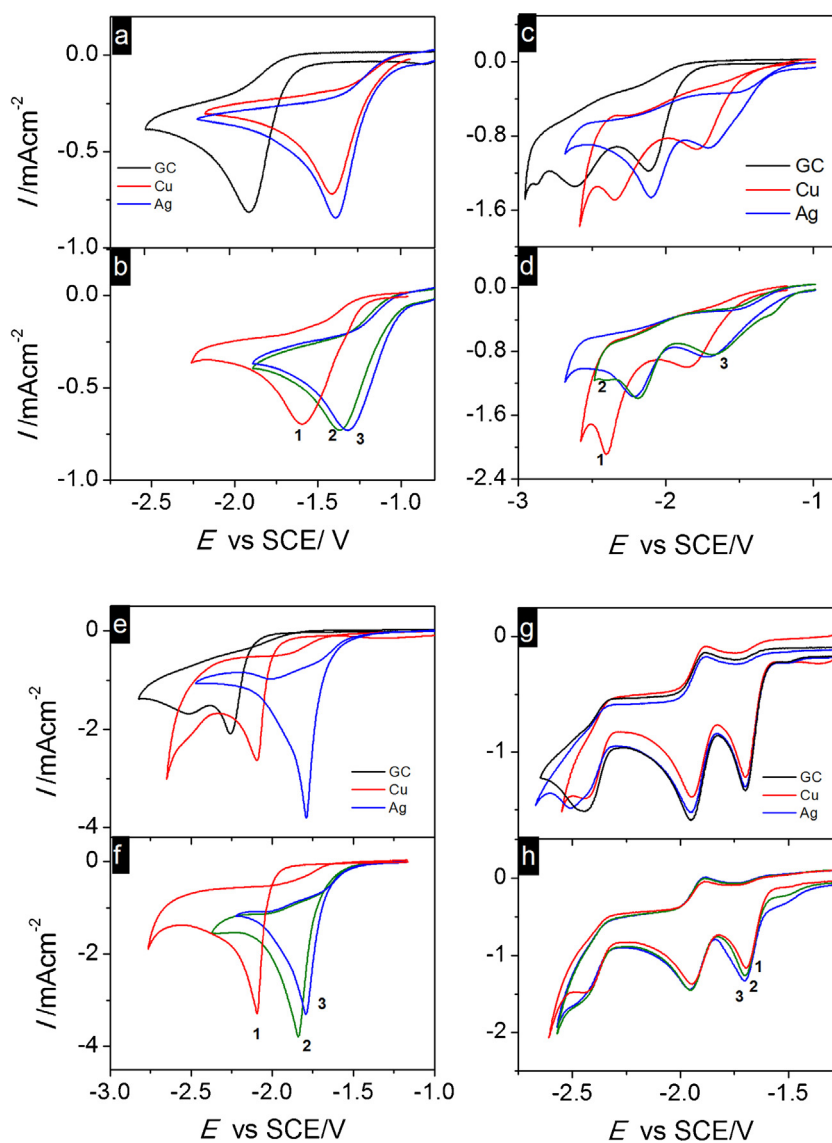


Fig. 7. Cyclic voltammetry of 2 mM: (a,b) chloroacetonitrile, (c,d) chloroform, (e,f) trichloroethylene, (g,h) chloroanthracene, in DMF + 0.1 M TEABF₄ at $\nu = 0.2 \text{ V s}^{-1}$ at different electrode surfaces: (a,c,e,g) GC, Ag, Cu; (b,d,f,h) CuNPs-GC (1), Ag150@CuNPs-GC (2) and Ag600@CuNPs-GC (3).

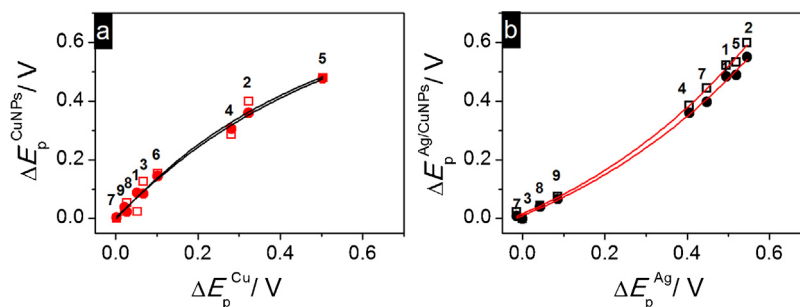


Fig. 8. Comparison of the positive shift of the reduction peak of RCI in DMF + 0.1 M TEABF₄ measured at $\nu = 0.2 \text{ V s}^{-1}$ (a) CuNPs-GC vs. bulk Cu (full marks 20 s, empty marks 30 s); (b) Ag150@CuNPs-GC (full marks) and Ag600@CuNPs-GC (empty marks) vs. bulk Ag.

β -elimination of chlorine atoms, where 2Cl^- are expelled and a triple bond is formed. The so generated chloroacetylene can be further reduced to acetylene which is the main product [64]. Trichloroethylene has a low lying π^* orbital in which the incoming electron can be initially accommodated. The kinetic indicator κ determined for GC and bulk metals are in line with a step-wise DET, on the contrary the nanostructured electrodes show $\kappa \ll 0.5$ that would be indicative of a concerted DET. In the case of trichloroethylene, the determination of ET coefficient is heavily affected by adsorption phenomena, which may influence the correct determination of κ values from both $\partial E_p / \partial \log \nu$ and peak width. The adsorption processes are visible as sharp peaks in the cyclic voltammetry reported in Fig. 7 e and f. Therefore we retain that in this case the determined κ values are poorly reliable. Whether the reduction of trichloroethylene follows a concerted or a step-wise mechanism, a catalytic activity was observed at CuNPs-GC, Ag150@CuNPs-GC and Ag600@CuNPs-GC. In this case the calculated ΔE_p are comparable but not better than those recorded on bulk Ag and Cu (Tables 2 and 3).

Compounds (7–9) are aromatic chlorides able to delocalize an electron on π^* orbitals. As reported in Table 2, the kinetic indicator $\kappa > 0.5$, which establishes that the reductive cleavage of C–X bond in the three aromatic molecules occurs according to a step-wise mechanism, where the bond breaking (Eq. (8)) is the prevalent controlling step. These compounds show comparable electrochemical behaviour at all investigated electrodes; this stems the absence of an electrode material effect on the electrochemical reduction mechanism. The cyclic voltammetry of chloroanthracene is reported, as representative example, in Fig. 7 g and h. Comparison of the peak potentials, E_p , obtained at the different electrodes (Tables 2 and 3) shows no catalytic effect at both Cu and Ag/Cu nanostructured electrodes [65].

Data reported here show that Ag/Cu NPs and to a lesser extent Cu NPs have good electrocatalytic properties for several types of organic chlorides. Fig. 8 reports the comparison of the electrocatalytic activities of Cu NPs and Ag/Cu NPs with those of the bulk metals. In Fig. 8a, ΔE_p measured at $\nu = 0.2 \text{ V s}^{-1}$ at CuNPs-GC, $\Delta E_p^{\text{CuNPs}}$, are plotted versus ΔE_p values obtained at bulk Cu at the same scan rate. As clearly shown, the investigated compounds are for the main part gathered at low values indicating a limited catalytic activity of both bulk and nanostructured copper electrodes. It is interesting to note that the plot follows a concave function and this can be tentatively interpreted as a general tendency for the Cu nanostructured electrode to be more catalytic than bulk Cu towards the reduction of organic chlorides. However, a more accurate evaluation of the ΔE_p reported in Tables 2 and 3 indicates that this is only partially true. In fact, among the six compounds following concerted DET a better performance at CuNPs-GC with respect to bulk Cu is observed for (1), (2) and (6). This indicates that thought a particle size effect is present at Cu electrodes,

it cannot be univocally correlated on the basis of the sole molecular structure, number of chloride atoms or reduction mechanism. In particular polychloromethanes (3–5) seem to be less influenced by the nanostructuration of the electrode with respect to mono-chlorinated compound such as chloroacetonitrile or benzylchloride.

Fig. 8b shows ΔE_p measured at Ag150@CuNPs-GC and Ag600@CuNPs-GC, $\Delta E_p^{\text{Ag/CuNPs}}$, plotted versus ΔE_p measured at bulk Ag. In this case, all compounds following a concerted mechanism are gathered at high values indicating that there is an excellent catalytic activity for both nanostructured electrodes. In this case the plot fitting the experimental data is a convex function and this indicates that Ag bulk generally performs better than Ag/Cu nanostructured electrodes in the dechlorination process. Thus, to resume it can be asserted that only a small particle size effect is present passing from bulk to nanostructured electrodes and that this effect is more visible in the case of low active material, as it is Cu.

4. Conclusions

We have shown that Cu NPs can be successfully deposited on a GC substrate by a double step potentiostatic deposition, obtaining NPs of average dimension of 20 to 40 nm depending on the deposition time. The same NPs can be modified by displacement deposition with silver, obtaining mixed agglomerates of Ag and Cu, where, on the basis of EDX results, Cu remains the predominant core component and the deposited Ag remains confined on the NPs surface. This procedure allows to obtain a Ag/Cu nanostructured electrode with high exposed Ag surface, while keeping low the metal loading so that the surface area/metal loading ratio is sensibly improved. Cu and Ag/Cu NPs have shown good electrocatalytic properties toward the reductive cleavage of carbon–chloride bonds. In particular, Cu and Ag/Cu NPs have been tested toward the reduction of benzyl chloride and they have shown to behave even better than bulk electrodes, notwithstanding a low content of active phase. A whole series of organic chlorides with different molecular structures and multiple C–Cl bonds have been examined. It has been shown that the catalytic activity of nanostructured electrodes is not limited to only few compounds, but, as long as organic chloride follows a concerted DET mechanism, there is good electrocatalysis. In all cases nanostructured electrodes have comparable catalytic properties with respect to bulk electrodes and in some cases the catalytic activity results even better. The better performances have been recorded on monochlorinated compounds such as benzyl chloride or chloroacetonitrile, while the catalytic effect tends to decrease on the increase of the number of C–Cl bonds. Furthermore, the mixed agglomerates of Ag and Cu NPs has shown a more reproducible behaviour than the sole Cu NPs and this is possibly due to the presence of Ag which hampers the oxidation of the exposed Cu NPs.

Acknowledgments

We gratefully acknowledge financial support from the University of Padova. MF acknowledges Fondazione Cariparo for financial support.

References

- [1] X.F. Wu, P. Anbarasan, H. Neumann, M. Beller, *Angew. Chem. Int. Ed.* 49 (2010) 9047–9050.
- [2] R.N. Dhital, C. Kamonsatikul, E. Somsook, K. Bobuatong, M. Ehara, S. Karanjit, H. Sakurai, *J. Am. Chem. Soc.* 134 (2012) 20250–20253.
- [3] A.A. Isse, C. Durante, A. Gennaro, *Electrochem. Commun.* 13 (2011) 810–813.
- [4] C. Durante, A.A. Isse, F. Todesco, A. Gennaro, *J. Electrochem. Soc.* 160 (2013) G3073–G3079.
- [5] F. Bellesia, A.J. Clark, F. Felluga, A. Gennaro, A.A. Isse, F. Roncaglia, F. Ghelfi, *Adv. Synth. Catal.* 355 (2013) 1649–1660.
- [6] A.H.E. Muller, K. Matyjaszewski, *Controlled and Living Polymerizations Methods and Materials*, WILEY-VCH Verlag GmbH & Co. KGaA, Weinheim, 2009.
- [7] A.J.D. Magenau, N.C. Strandwitz, A. Gennaro, K. Matyjaszewski, *Science* 332 (2011) 81–84.
- [8] V.V. Lunin, E.S. Lokteva, *Russ. Chem. Bull.* 45 (1996) 1519–1534.
- [9] Y. Xie, D.M. Cwiertny, *Environ. Sci. Technol.* 47 (2013) 7940–7948.
- [10] C. Scheutz, N.D. Durant, M.H. Hansen, P.L. Bjerg, *Water Res.* 45 (2011) 2701–2723.
- [11] T. Hennebel, S. De Corte, W. Verstraete, N. Boon, *Curr. Opin. Biotechnol.* 23 (2012) 555–561.
- [12] B. Huang, C. Durante, A.A. Isse, A. Gennaro, *Electrochem. Commun.* 34 (2013) 90–93.
- [13] M.J. Medeiros, C.S.S. Neves, A.R. Pereira, E. Dunăch, *Electrochim. Acta* 56 (2011) 4498–4503.
- [14] B. Huang, A.A. Isse, C. Durante, C. Wei, A. Gennaro, *Electrochim. Acta* 70 (2012) 50–61.
- [15] O. Scialdone, A. Galia, C. Guarisco, S. La Mantia, *Chem. Eng. J.* 189–190 (2012) 229–236.
- [16] A.A. Isse, S. Gottardello, C. Maccato, A. Gennaro, *Electrochem. Commun.* 8 (2006) 1707.
- [17] L.M. Strawsine, M.S. Mubarak, D.G. Peters, *J. Electrochem. Soc.* 160 (2013) G3030–G3037.
- [18] A.A. Pevery, J.A. Karty, D.G. Peters, *J. Electroanal. Chem.* 692 (2013) 66–71.
- [19] C. Durante, A.A. Isse, G. Sandonà, A. Gennaro, *Appl. Catal., B: Environ.* 88 (2009) 479–489.
- [20] A.A. Isse, B. Huang, C. Durante, A. Gennaro, *Appl. Catal., B: Environ.* 126 (2012) 347–354.
- [21] C. Durante, B. Huang, A.A. Isse, A. Gennaro, *Appl. Catal., B: Environ.* 126 (2012) 355–362.
- [22] J. Simonet, *J. Electroanal. Chem.* 632 (2009) 30–38.
- [23] L. Perini, C. Durante, M. Favaro, S. Agnoli, G. Granozzi, A. Gennaro, *Appl. Catal., B: Environ.* 144 (2014) 300–307.
- [24] A.A. Isse, S. Gottardello, C. Durante, A. Gennaro, *Phys. Chem. Chem. Phys.* 10 (2008) 2409–2416.
- [25] V. Jouikov, J. Simonet, *Electrochem. Commun.* 12 (2010) 331–334.
- [26] P. Poizot, J. Simonet, *Electrochim. Acta* 56 (2010) 15–36.
- [27] S. Rondinini, G. Aricci, Ž. Krpetić, C. Locatelli, A. Minguzzi, F. Porta, A. Vertova, *Fuel Cells* 3 (2009) 253–263.
- [28] T. Maiyalagan, *Appl. Catal., A: Gen.* 340 (2008) 191–195.
- [29] J. Saelim, P. Kanatharana, P. Thavarungkul, C. Thammakhet, *Microchem. J.* 108 (2013) 180–187.
- [30] A. Minguzzi, O. Lugaresi, G. Aricci, S. Rondinini, A. Vertova, *Electrochem. Commun.* 22 (2012) 25–28.
- [31] A. Gennaro, A.A. Isse, C.L. Bianchi, P.R. Mussini, M. Rossi, *Electrochem. Commun.* 11 (2009) 1932–1935.
- [32] N.L. Pocard, D.C. Alsmeyer, R.L. McCreery, T.X. Neenan, M.R. Callstrom, *J. Mater. Chem.* 2 (1992) 771–784.
- [33] M. Fedurco, J. Sartoretti, J. Augustynski, *Langmuir* 17 (2001) 2380–2387.
- [34] M. Fedurco, L. Coppex, J. Augustynski, *J. Phys. Chem. B* 106 (2002) 2625–2633.
- [35] C.H. Tsai, S.Y. Chen, J.M. Song, I.G. Chen, H.Y. Lee, *Corros. Sci.* 74 (2013) 123–129.
- [36] Z. Chen, D. Mochizuki, M.M. Maitani, Y. Wada, *Nanotechnology* 24 (2013) 265602–265611.
- [37] A.A. Isse, G. Sandonà, C. Durante, A. Gennaro, *Electrochim. Acta* 54 (2009) 3235–3243.
- [38] L. Falciola, A. Gennaro, A.A. Isse, P.R. Mussini, M. Rossi, *J. Electroanal. Chem.* 593 (2006) 47–56.
- [39] A. Milchev, T. Zapryanova, *Electrochim. Acta* 51 (2006) 2926–2933.
- [40] A. Milchev, T. Zapryanova, *Electrochim. Acta* 51 (2006) 4916–4921.
- [41] T. Zapryanova, A. Hrussanova, A. Milchev, *J. Electroanal. Chem.* 600 (2007) 311–317.
- [42] L. Bonou, M. Eyraud, J. Crousier, *J. Appl. Electrochem.* 24 (1994) 906–910.
- [43] D. Grujicic, B. Pesic, *Electrochim. Acta* 47 (2002) 2901–2912.
- [44] C.R. Henry, *Prog. Surf. Sci.* 80 (2005) 92–116.
- [45] A. Radi, D. Pradhan, Y. Sohn, K.T. Leung, *ACS Nano* 4 (2010) 1553–1560.
- [46] D.L. Lu, K.I. Tanaka, *J. Phys. Chem. B* 101 (1997) 4030–4034.
- [47] V. Mancier, C. Rousse-Bertrand, J. Dille, J. Michel, P. Fricoteaux, *Ultrason. Sonochem.* 17 (2010) 690–696.
- [48] J. Zhao, D. Zhang, X. Song, *Appl. Surf. Sci.* 258 (2012) 7430–7434.
- [49] K.L. Yeung, S.C. Christiansen, A. Varma, *J. Membrane Sci.* 159 (1999) 107–122.
- [50] C. Ratsch, A.P. Seitsonen, M. Scheffler, *Phys. Rev. B: Condens. Matter* 55 (1997) 6750–6753.
- [51] C.D. Wagner, *Anal. Chem.* 44 (1972) 967–973.
- [52] C.D. Wagner, *Faraday Discuss. Chem. Soc.* 60 (1975) 291–300.
- [53] C.D. Wagner, L.H. Gale, R.H. Raymond, *Anal. Chem.* 51 (1979) 466–482.
- [54] G. Moretti, *J. Electron Spectrosc. Relat. Phenom.* 95 (1998) 95–144.
- [55] K. Luo, X. Lai, C.W. Yi, K.A. Davis, K.K. Gath, D.W. Goodman, *J. Phys. Chem. B* 109 (2005) 4064–4068.
- [56] J.Y. Wang, J. DuPlessis, J.J. Terblans, G.N. Van Wyk, *Surf. Sci.* 419 (1999) 197–206.
- [57] R. Vasilic, L.T. Viyannalage, N. Dimitrov, *J. Electrochem. Soc.* 153 (2006) C648–C655.
- [58] L.T. Viyannalage, R. Vasilic, N. Dimitrov, *J. Phys. Chem. C* 111 (2007) 4036–4041.
- [59] A. Hernandez-Creus, P. Carro, S. Gonzalez, R.C. Salvarezza, A.J. Arvia, *J. Electrochem. Soc.* 139 (1992) 1064–1070.
- [60] E. Kirowa Eissner, Y. Bonfil, D. Tzur, E. Gileadi, *J. Electroanal. Chem.* 552 (2003) 171–183.
- [61] J.-M. Savéant, *Elements of Molecular and Biomolecular Electrochemistry*, Wiley-Interscience, New York, NY, 2006.
- [62] A.A. Isse, P.R. Mussini, A. Gennaro, *J. Phys. Chem. C* 113 (2009) 14983–14992.
- [63] A.J. Bard, L.R. Faulkner, *Electrochemical Methods*, second ed., John Wiley & Sons, New York, NY, 2001.
- [64] C. Durante, A.A. Isse, A. Gennaro, *J. Appl. Electrochem.* 43 (2013) 227–235.
- [65] A.A. Isse, L. Falciola, P.R. Mussini, A. Gennaro, *Chem. Commun.* (2006) 344–346.